SUPPLEMENTARY INFORMATION

doi:10.1038/nature09933

THEORY OF OPTOMECHANICAL EIT, EIA AND PARAMETRIC AMPLIFICATION

Here we provide a theoretical treatment of some of the main aspects of EIT [1–4], EIA [5] and parametric amplification [6–8] in optomechanical systems. Modeling the optomechanical system with the Hamiltonian

$$\hat{H} = \hbar\omega_o \hat{a}^\dagger \hat{a} + \hbar\omega_m \hat{b}^\dagger \hat{b} + \hbar g(\hat{b}^\dagger + \hat{b})\hat{a}^\dagger \hat{a} + i\hbar\sqrt{\frac{\kappa_{\rm ex}}{2}}\alpha_{{\rm in},0} e^{-i\omega_{\rm c} t}(\hat{a} - \hat{a}^\dagger), \tag{S1}$$

it is possible to linearize the operation of the system, under the influence of a control laser at $\omega_{\rm c}$, about a particular steady-state given by intracavity photon amplitude α_0 and a static phonon shift β_0. The interaction of the mechanics and pump photons at $\omega_{\rm c}$ with secondary "probe" photons at $\omega_s = \omega_{\rm c} \pm \Delta$ with two-photon detuning Δ can then be modeled by making the substitutions

$$\hat{a} \to \alpha_0 e^{-i\omega_{\rm c} t} + (\alpha_- e^{-i(\omega_{\rm c}+\Delta)t} + \alpha_+ e^{-i(\omega_{\rm c}-\Delta)t}), \qquad \hat{b} \to \beta_0 + \beta_- e^{-i\Delta t}. \tag{S2}$$

Assuming that the pump is much larger than the probe, $|\alpha_0| \gg |\alpha_\pm|$, the pump amplitude is left unaffected and the equations for each sideband amplitude $\alpha_\pm$ are found to be

$$\pm i\omega\alpha_\pm = -\left(i\Delta_{\rm OC} + \frac{\kappa}{2}\right)\alpha_\pm - ig\alpha_0\beta_\pm - \sqrt{\frac{\kappa_{\rm ex}}{2}}\alpha_{{\rm in},\pm}, \tag{S3}$$

$$-i\omega\beta_- = -\left(i\omega_m + \frac{\gamma_i}{2}\right)\beta_- - ig(\alpha_0^*\alpha_- + \alpha_0\alpha_+^*) - \sqrt{\gamma_i}\beta_{{\rm in},-}. \tag{S4}$$

We have defined $\Delta_{\rm OC} = \omega_o' - \omega_{\rm c}$ as the pump detuning from the optical cavity (including the static optomechanical shift, ω_o'), and $\beta_+ = \beta_-^*$. In these situations it is typical to define $G = g\alpha_0$, as the effective optomechanical coupling rate between a sideband and the mechanical subsystem, mediated by the pump.

Red-detuned pump: Electromagnetically Induced Transparency

With the pump detuned from the cavity by a two-photon detuning Δ, the spectral selectivity of the optical cavity causes the sideband populations to be skewed in a drastic fashion. It is then an acceptable approximation to neglect one of these sidebands, depending on whether the pump is on the red or blue side of the cavity. When the pump resides on the red side ($\Delta_{\rm OC} > 0$), the α_+ is reduced and can be neglected. This is the rotating wave approximation (RWA) and is valid so long as $\Delta \gg \kappa$.

Then Eqs. (S3-S4) may be solved for the reflection and transmission coefficients $r(\omega_s)$ and $t(\omega_s)$ of the side-coupled cavity system. We find that

$$r(\Delta) = -\frac{\kappa_{\rm ex}/2}{i(\Delta_{\rm OC} - \Delta) + \kappa/2 + \frac{|G|^2}{i(\omega_m - \Delta) + \gamma_i/2}} \tag{S5}$$

$$t(\Delta) = 1 - \frac{\kappa_{\rm ex}/2}{i(\Delta_{\rm OC} - \Delta) + \kappa/2 + \frac{|G|^2}{i(\omega_m - \Delta) + \gamma_i/2}}. \tag{S6}$$

These equations are plotted in Figs. S1 and S2.

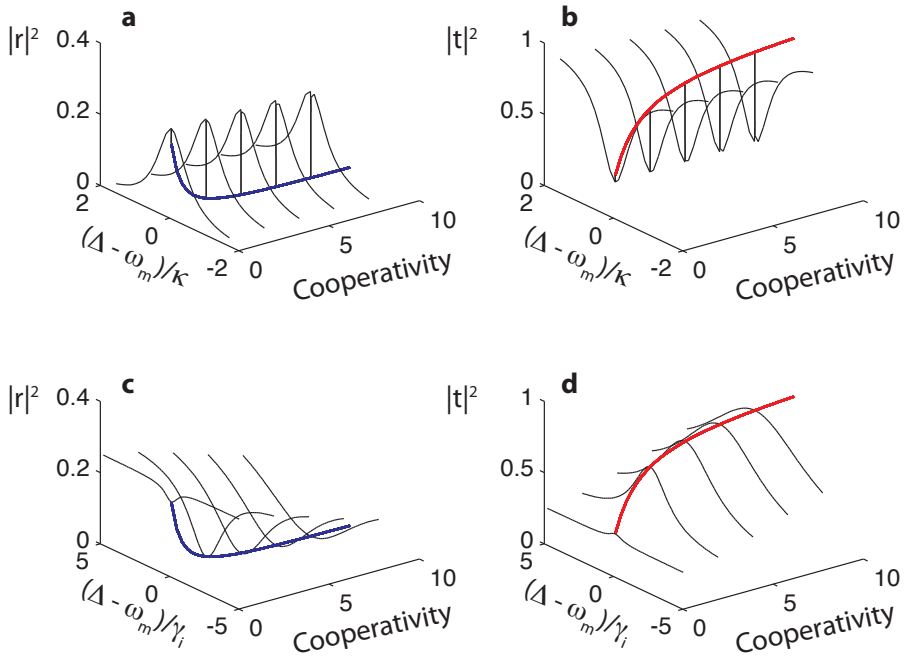

FIG. S1: **Electromagnetically Induced Transparency Spectra. a, c,** The reflected signal amplitude, as a function of two-photon detuning Δ for the case where $\Delta_{\rm OC} = \omega_m$. In **b, d,** the corresponding plots for transmission are shown. The broadening of the transmission window, and the saturation of the transmission peak, and reflection dip are evident in **c, d** respectively.

Group Delay

For the red-detuned system, the existence of an effective transparency on transmission makes the group delay imparted on the pulse an interesting quantity. To calculate the reflection and transmission group delays we consider a pulse

$$f(t_o) = \int_0^\infty f(\omega) e^{-i\omega t_o} \mathrm{d}\omega, \tag{S7}$$

where most of the spectrum is confined to a small window ($< 4G^2/\kappa$) about a central signal frequency ω_s. Then the transmitted signal $f^{(\mathrm{T})}(t_o)$ may be written as

$$\begin{aligned} f^{(\mathrm{T})}(t_o) &= \int_0^\infty t(\omega) f(\omega) e^{-i\omega t_o} \mathrm{d}\omega \\ &= e^{-i\omega_s t_o} \int_{-\infty}^\infty t(\omega_s+\delta) f(\omega_s+\delta) e^{-i\delta t_o} \mathrm{d}\delta \\ &= e^{-i\omega_s t_o} \int_{-\infty}^\infty t(\omega_s) \left(1 + \frac{1}{t(\omega_s)} \left.\frac{\mathrm{d}t}{\mathrm{d}\omega}\right|_{\omega_s} \delta + o(\delta^2)\right) f(\omega_s+\delta) e^{-i\delta t_o} \mathrm{d}\delta \\ &\approx e^{-i\omega_s t_o} \int_{-\infty}^\infty t(\omega_s) f(\omega_s+\delta) e^{-i\delta(t_o - \tau^{(\mathrm{T})})} \mathrm{d}\delta \end{aligned} \tag{S8}$$

The last line implies that $f^{(\mathrm{T})}(t_o) \approx f(t_o - \tau^{(\mathrm{T})})$, where

$$\tau^{(\mathrm{T})} = \mathcal{R}\left\{ \frac{-i}{t(\omega_s)} \frac{\mathrm{d}t}{\mathrm{d}\omega} \right\}. \tag{S9}$$

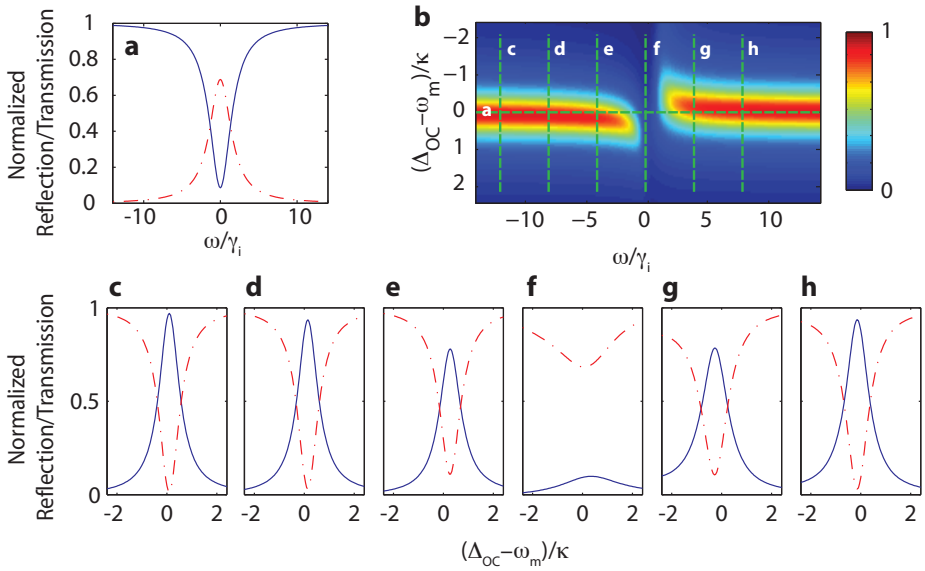

FIG. S2: **a**, normalized reflection (solid blue line) and transmission (dot-dash red line) signal for $\Delta_{\rm OC} = \omega_m$ versus the normalized two-photon detuning frequency (Δ/γ_i). **b** normalized reflection signal map as a function of the normalized pump detuning ($(\Delta_{\rm OC}-\omega_m)/\kappa$) and the normalized two-photon detuning frequency. Each dashed line corresponds to the curves shown in **a, c-h**. **c-h** normalized reflection (solid blue line) and transmission (dot-dash red line) signals as a function of normalized pump detuning. Each curve again corresponds to a specific two-photon detuning, as designated in b. For **f**, $\Delta \approx \omega_m$, then the reflected signal is pratically zero on the vicinity of the resonance condition $\Delta_{\rm OC} = \omega_m$.

The reflection group delay may also be defined analogously,

$$\tau^{(\rm R)} = \mathcal{R}\left\{\frac{-i}{r(\omega_s)}\frac{{\rm d}r}{{\rm d}\omega}\right\}. \tag{S10}$$

With the signal sent at a two-photon detuning $\Delta = \omega_m$, we find

$$\tau^{(\rm T)}|_{\Delta=\omega_m} = \frac{2}{\gamma_i}\frac{(\kappa_e/\kappa)C}{(1+C)(1-(\kappa_e/\kappa)+C)}, \tag{S11}$$

where the cooperativity $C = 4G^2/\kappa\gamma_i$ is a measure of the coupling between the mechanical oscillator and the optical bath. Under the same conditions we find that group delay for reflection is given by

$$\tau^{(\rm R)}|_{\Delta=\omega_m} = -\frac{2}{\gamma_i}\frac{C}{1+C}, \tag{S12}$$

resulting in the limit $C \gg 1$

$$\tau^{(\rm T)}|_{\Delta=\omega_m} \to \frac{2}{\gamma_i}\frac{\kappa_e}{\kappa}\frac{1}{C} \qquad \text{and} \qquad \tau^{(\rm R)}|_{\Delta=\omega_m} \to -\frac{2}{\gamma_i}. \tag{S13}$$

A quantity of interest, the delay-bandwidth product can be calculated for the transmitted signal, by taking the product of the signal delay $|\tau^{(\rm T)}|_{\rm max}$, and the bandwidth $\Delta\omega = \gamma_i C$, to give us $\Delta\omega \cdot t_d = 2(\kappa_e/\kappa)$.

Using equations S11 and S5 we can estimate the maximum delay for our system. The reflection and transmission coefficients at resonance ($\Delta = \Delta_{\rm OC} = \omega_m$)) are given by

$$r_{\rm max} = -\frac{(\kappa_e/\kappa)}{1+C} \qquad \text{and} \qquad t_{\rm max} = \frac{1-(\kappa_e/\kappa)+C}{1+C}. \tag{S14}$$

For the case where intrinsic optical losses are negligible, i.e. $\kappa_e = \kappa$, the equations for delay and transmission coefficient contrast can be written as

$$t_{\rm max} = \frac{C}{1+C}, \qquad \tau^{(\rm T)}_{\rm max} = \frac{2}{\gamma_i}\frac{1}{(1+C)}, \tag{S15}$$

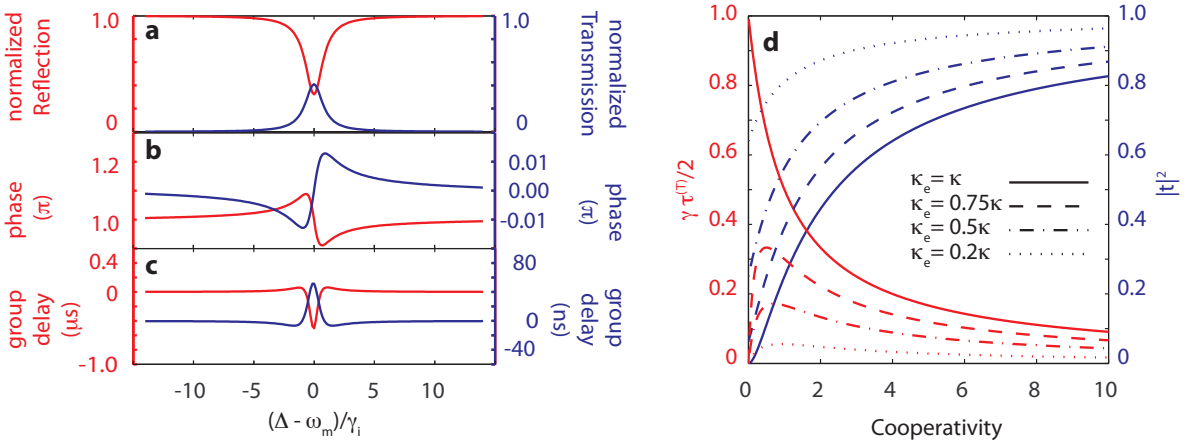

FIG. S3: **Phase and Group Delay in EIT. a,** Normalized reflection (red) and transmission (blue) signals, with the phase **b**, and group delay **c**, for typical system parameters. **d,** Maximum delay ($\tau^{(T)}_{\max}$), in units of $\gamma_i/2$, and transmission coefficient ($|t_{\max}|^2$) for the transmitted signal as a function of the cooperativity for different cavity-waveguide couplings.

and are plotted in Fig. S3.

Blue-detuned pump: Electromagnetically Induced Absorption and Amplification

By placing the pump at a mechanical frequency away from cavity, on the blue side ($\Delta_{\rm OC} = -\omega_m$) we may ignore the α_- sideband of the intracavity photons. The reflection in this case is calculated to be

$$r_{\rm A}(\omega_s) = -\frac{\kappa_{\rm ex}/2}{i(\Delta_{\rm OC}+\Delta)+\kappa/2+\frac{|G|^2}{i(\omega_m-\Delta)-\gamma_i/2}} \tag{S16}$$

and $t_{\rm A}(\omega_s) = 1 + r_{\rm A}(\omega_s)$. The linearization which leads to this equation from the full dynamics of the system, only holds below the phonon lasing threshold, $C = 1$, and so we limit ourselves to the case where $C < 1$. The effective interaction Hamiltonian of the system which is obtained after making the rotating wave approximation to remove terms counter-rotating at the mechanical frequency, is given by [9]

$$H_{\rm int} = \hbar G(\hat{a}^\dagger \hat{b}^\dagger + \hat{a}\hat{b}). \tag{S17}$$

This is also the Hamiltonian of a parametric oscillator, whose quantum theory has been known for some time [6, 8]. The only distinction with our system, is that we consider and measure mainly the reflection and transmission properties of the parametric oscillator, as opposed to its internal dynamics. Using the expression in eqn. (S16) we find

$$r_{\max} = -\frac{(\kappa_e/\kappa)}{1-C} \qquad \text{and} \qquad t_{\max} = \frac{1-(\kappa_e/\kappa)-C}{1-C}. \tag{S18}$$

These expressions are plotted in Fig S4a-d for a range of cooperativities. The ratio between the power leaving the cavity through the waveguide to the input power is the sum of the reflection and transmission coefficient amplitudes, $p = |t_{\max}|^2 + |r_{\max}|^2$. As the base-line value, we take $C = 0$ for which the emitted power is $p_0 = (\kappa_e/\kappa)^2 + (\kappa_i/\kappa)^2$.

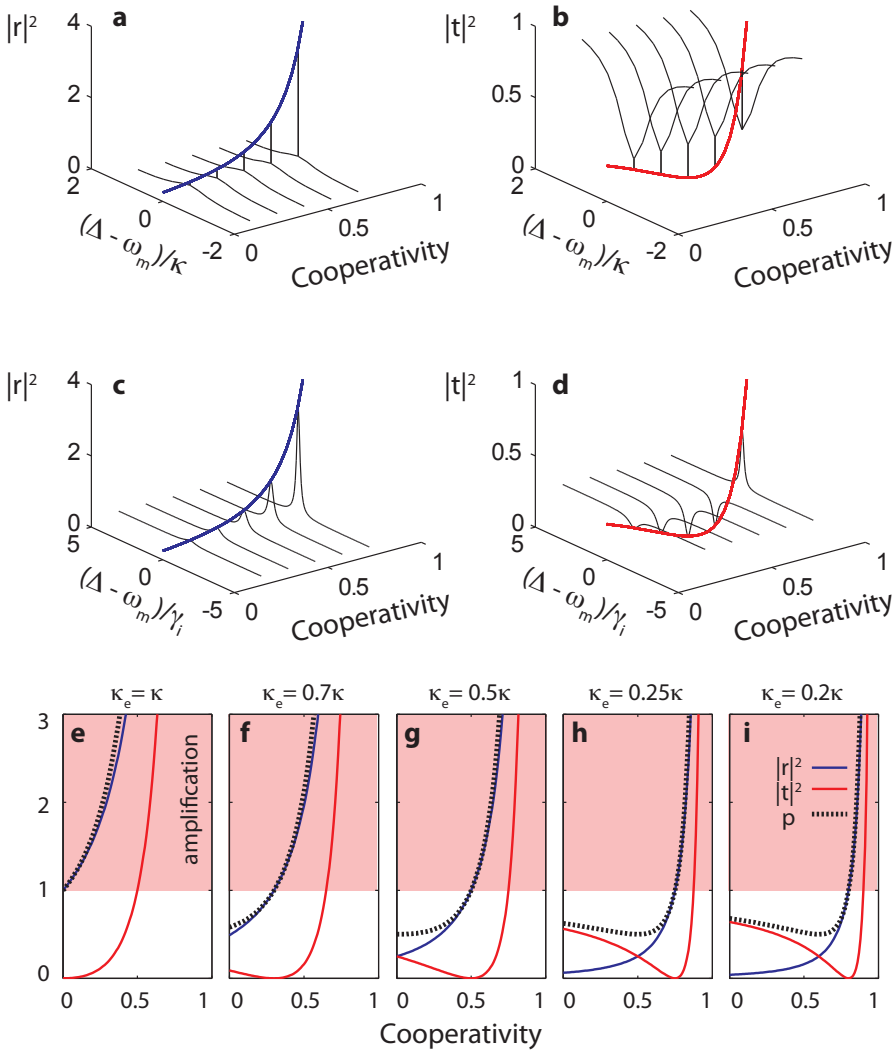

FIG. S4: **Electromagnetically Induced Absorption and Amplification Spectra. a, c,** The reflected signal amplitude, as a function of two-photon detuning Δ for the case where $\Delta_{OC} = -\omega_m$. In **b, d,** the corresponding plots for transmission are shown. The increase in the reflected signal is evident in **a,c**. In **b,d** we see a reduction in the transmitted signal amplitude, down to zero, and followed by an increase. **e-i** The amplitude of the reflected (blue), transmitted (red) and total power (dashed black) from the cavity, for various cavity-waveguide coupling efficiencies. The region where $|r|^2, p > 1$ is called the amplification region, and shaded. Note that for $\kappa_e < \kappa/2$, the power from the cavity is at first reduced with higher cooperativity, before increasing and going into the amplification regime at $C > 1-\kappa_e/\kappa$. This corresponds to electromagnetically induced absorption.

Weak-Coupling: Electromagnetically Induced Absorption

At small cooperativities $C \ll 1$ and weak cavity-waveguide coupling $\kappa_e < \kappa_i$, the behaviour of our system is analogous to what has been observed in atomic gases, and been called Electromagnetically Induced Absorption (EIA) [5]. Under these conditions, p is less than p_0, and more of the incoming photons are now absorbed than in the case with $C = 0$. As such, the reflection will exhibit an absorption peak, and the transmission an absorption dip. As long as $\kappa_e < \kappa_i$, there will always be a value of C such that absorption is enhanced, as experimentally demonstrated

in this paper. In systems where $\kappa_e > \kappa_i$, we find $p > p_0$ for any finite C. Plots of the transmission, reflection, and p are shown as a function of cooperativity in Fig. S4e-i. It can be seen that the slope of p at $C = 0$ goes from positive to negative as κ_i over-takes κ_e. Even with weak cavity-waveguide coupling, at sufficiently high C, the system changes from absorptive to amplifying with p becoming much larger than p_0 and 1, as can be seen in the shaded region of Fig. S4e-i.

Amplification

As suggested by the effective Hamiltonian of the system in eqn. (S17), parametric amplification ($p > 1$) is always possible, and occurs at $C > 1 - (\kappa_e/\kappa)$. It is important to note that at perfect coupling, $\kappa_e = \kappa$, amplification will occur for any finite C. This can be seen in Fig. S4, which shows that the transmission is always greater than unity for finite C.

Group Delay

Following a derivation similar to that in the previous section we arrive at values for maximum group delay $\tau_A^{(\mathrm{T})}|_{\max}$, $\tau_A^{(\mathrm{R})}|_{\max}$ given by

$$\tau_A^{(\mathrm{R})}|_{\Delta=\omega_m} = -\frac{2}{\gamma_i}\frac{C}{1-C}, \tag{S19}$$

$$\tau_A^{(\mathrm{T})}|_{\Delta=\omega_m} = \frac{2}{\gamma_i}\frac{\kappa_{\mathrm{ex}}}{\kappa}\frac{C}{(1-C)(1-\kappa_{\mathrm{ex}}/\kappa-C)}. \tag{S20}$$

Note that as C increases, and the system switches at $C = 1 - \kappa_e/\kappa$ from absorptive to amplifying, and the sign of the group delay on transmission changes from from positive to negative. For systems with strong cavity-waveguide coupling, $\kappa_e \approx \kappa$, both $\tau_A^{(\mathrm{R})}|_{\Delta=\omega_m}$ and $\tau_A^{(\mathrm{T})}|_{\Delta=\omega_m}$ are negative, pointing to causality-preserving superluminal light.

FABRICATION

The nano-beam cavities were fabricated using a Silicon-On-Insulator wafer from SOITEC (ρ = 4-20 Ω·cm, device layer thickness t = 220 nm, buried-oxide layer thickness 2 μm). The cavity geometry is defined by electron beam lithography followed by inductively-coupled-plasma reactive ion etching (ICP-RIE) to transfer the pattern through the 220 nm silicon device layer. The cavities were then undercut using HF:H_2O solution to remove the buried oxide layer, and cleaned using a piranha/HF cycle [10]. The dimensions and design of the nano-beam will be discussed in details elsewhere.

DATA MEASUREMENT AND ANALYSIS

Experimental Setup

The detailed experimental setup used to measure the EIT window and delay properties of the optomechanical crystal is shown in Fig. S5(a). The setup is designed to record simultaneously the reflected signals from a probe sideband while scanning and recording the pump laser transmission.

As a light source we use a fiber-coupled tunable infrared laser, (New Focus Velocity, model TLB-6328) spanning approximately 60 nm, centered around 1550 nm, which has its intensity controlled by a variable optical attenuator (VOA). A small percentage (10%) of the laser intensity is sent to a custom-made fiber coupled Mach-Zehnder (MZ) interferometer and has its intensity detected by a photodetector (Det.4, New Focus Nanosecond Photodetector, model 1623) for further wavelength calibration. To minimize polarization dependent losses on the electro-optical-modulator (EOM), a fiber polarization controller (FPC) is placed before it.

The AC signal used for the electro-optical modulator (EOM) comes from the radio-frequency signal generator (RF S.G., Rohde-Schwarz, SMA-100A). There, a rf-signal carrier at the two-photon detuning frequency ($\Delta/2\pi \sim 4$GHz) has its amplitude modulated at the Lock-in detection frequency ($\omega_{\mathrm{LI}}/2\pi \approx 89$ kHz). As a result, the EOM modulation

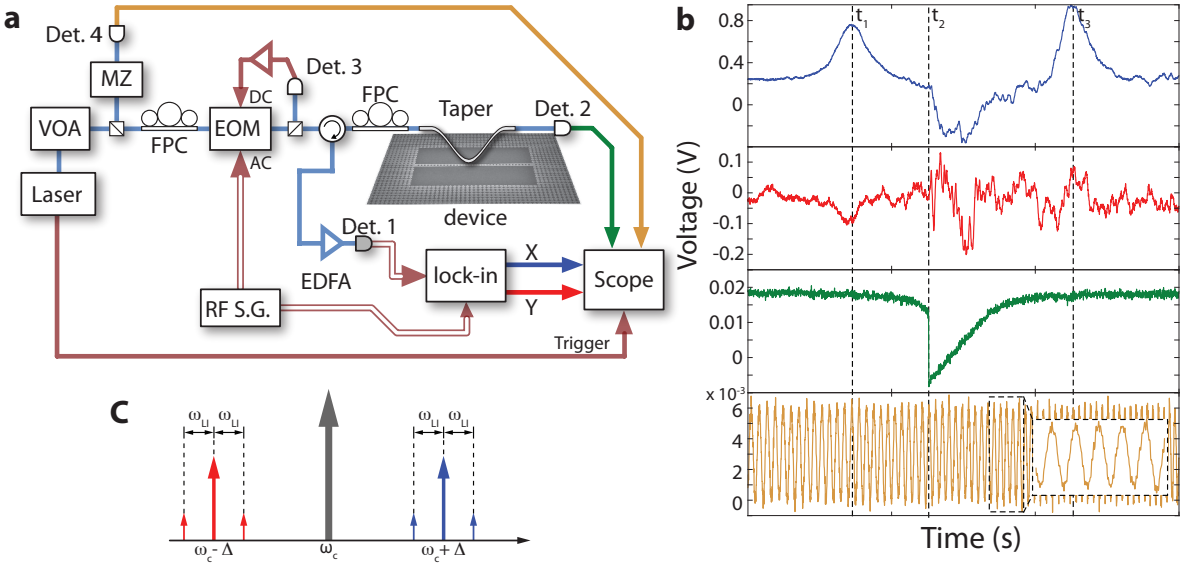

FIG. S5: **a**, Experimental setup. **b**, detected signals for data analysis. From top to bottom, the in phase (blue) and quadrature (red) lock-in signals from the reflected probe side band; the transmitted pump laser (green); and the Mach-Zehnder (MZ) amplitude signal (yellow) for wavelength calibration as explained on the text. **c**, schematic frequency domain spectra of the pump laser after the EOM. At t_1, the probe side band (blue detuned) is at $\omega_s = \omega_c + \Delta = \omega_o$, the cavity frequency while at t_3 the probe side band is at $\omega_s = \omega_c - \omega = \omega_o$.

produces two probe sidebands at Δ, where each of them have a small modulation at the lock-in frequency (see Fig. S5(c)).

A small portion of the signal from the EOM output (10%) is used (Det. 3) as a DC control signal to control for any low frequency power drift during the experiment, by keeping the EOM level locked. The remaining laser light is passed through a circulator, a FPC and then couple to a tapered and dimpled optical fiber (Taper) which has its position controlled with nanometer-scale precision (although vibrations and static electric forces limit the minimum stable spacing between the fiber and device to about 50 nm).

The transmitted light through the taper is detected (Det. 2) and recorded on the oscilloscope (Scope, Agilent, DSO80204B). Any reflected signal coming from the Taper/device is optically amplified by a Erbium-Doped-Fiber-Amplifier (EDFA) and detected by a high-speed photoreceiver (Det. 1, New Focus model, 1554-B) with a maximum transimpedance gain of $1,000$ V/A and a bandwidth (3 dB rolloff point) of 12 GHz. The rf-signal from the photoreceiver is sent to a Lock-in amplifier (L.I., SRS-830). The output from the in-phase and quadrature signals from the L.I. are also recorded on the same oscilloscope. The recorded signal on the oscilloscope is triggered by the sweeping frequency on the pump laser.

Since the pump is detuned from the cavity by $|\Delta_{\rm OC}| \gg \kappa$, it is filtered on reflection, while the modulated sidebands at $\omega_c \pm \Delta$ (where the sign is that of $\Delta_{\rm OC}$) are reflected and sent to a lock-in amplifier, where the component related to the modulated sideband is amplified and sent to an oscilloscope. Using a lock-in amplifier allows us to measure the phase-shift on the signal modulated at $\omega_{\rm LI}$, giving a direct measurement of the group delay imparted on the signal.

Fig. S2(b) shows a sample of the resulting raw data measured on the oscilloscope for the in-phase (blue curve) and out-phase (red curve) reflected signal detected by the lock-in amplifier; the pump transmission spectra (green curve); and the Mach-Zehnder interferometer pattern (yellow curve) used to calibrate the wavelength for the transmission and reflection data. The probe reflection is normalized based upon the transmission contrast for the pump laser at low input power, where the cavity line-shape is not distorted by thermal nonlinearities.

Data Analysis

Here we will show how the amplitude modulation of the signal sideband Δ is used to measure the reflection ($|r(\omega)|^2$) and delay ($\tau^{(\mathrm{R})}$) of the signal reflected from the cavity. The output of the EOM can be written as:

$$a_{\mathrm{out}}(t) = a_{\mathrm{in}}\left[1 + m\left(1 + m_{\mathrm{LI}}\cos(\omega_{\mathrm{LI}}t)\right)\cos(\Delta t)\right], \tag{S21}$$

where the input field amplitude $a_{\mathrm{in}}(t) = a_o\cos(\Delta t)$, $a_o = \sqrt{P_{\mathrm{in}}/\hbar\omega_{\mathrm{c}}}$, m is the EOM-modulation index and m_{LI} is amplitude modulation index on the rf signal at Δ. For the measurements shown in the main text $m_{\mathrm{LI}} = 1$. In this case one can write the field of the EOM output (cavity input) in the time domain as:

$$\begin{aligned} a_{\mathrm{out}}(t) &= a_o[\cos(\omega_c t) + \frac{m}{2}\left[\cos((\omega_{\mathrm{c}} + \Delta)t) + \cos((\omega_{\mathrm{c}} - \Delta)t)\right] \\ &+ \frac{m}{4}(\cos((\omega_{\mathrm{c}} + \Delta + \omega_{\mathrm{LI}})t) + \cos((\omega_{\mathrm{c}} + \Delta - \omega_{\mathrm{LI}})t)] \\ &+ \cos((\omega_{\mathrm{c}} - \Delta + \omega_{\mathrm{LI}})t) + \cos((\omega_{\mathrm{c}} - \Delta - \omega_{\mathrm{LI}})t))]. \end{aligned} \tag{S22}$$

Fig. S5(c) shows a schematic of the cavity input fields in the frequency domain. The reflected signal is filtered by the cavity dispersion and considering the case where the pump is on the red-side of the cavity ($\omega_{\mathrm{c}} < \omega_o$) the reflected field is:

$$a_R(t) = r(\omega_s)\frac{a_o\alpha}{4}\ \left[\cos((\omega_{\mathrm{c}} + \Delta)t) + \cos((\omega_{\mathrm{c}} + \Delta)t + (\omega_{\mathrm{LI}}t - \varphi)) + \cos((\omega_{\mathrm{c}} + \Delta)t - (\omega_{\mathrm{LI}}t - \varphi))\right] \tag{S23}$$

First we assume that $r(\omega)$ is roughly constant over a range of ω_{LI} which is true for $\omega_{\mathrm{LI}} < (\gamma_i + \gamma_{\mathrm{om}})/2$. This implies that the smallest transparency window we could measure is on the order of the lock-in detection frequency, which corresponds to the smallest input power for the low and room temperature data.

We can now write the time average detected power spectral density on the photoreceiver (Det. 1 on Fig. S5a) by taking the absolute square value of the reflected field and keeping only the terms with frequency smaller than the detector bandwidth. In this case:

$$P|_{\omega_s} = \frac{a_o^2\alpha^2 R_{PD}G_{PD}}{8R_L}|r(\omega_s)|^2\left[3 + 4\cos(\omega_{\mathrm{LI}}t - \varphi) + \frac{1}{2}\cos(2\omega_{LI}t - 2\varphi) + \mathcal{O}(2\omega_{\mathrm{c}})\right].$$

where $R_{PD} = 0.6$ A/V is the detector responsivity, $G_{PD} = 1000$ V/A is the detector gain and $R_L = 50\ \Omega$ is the load resistance.

This signal is then sent to the lock-in which can measure independently the in-phase (X) and quadrature (Y) power spectral densities at ω_{LI}:

$$X|_{\omega_{\mathrm{LI}}} = \frac{a_o^2\alpha^2 R_{PD}G_{PD}}{4R_L}|r(\omega_s)|^2\cos(\varphi)$$

$$Y|_{\omega_{\mathrm{LI}}} = \frac{a_o^2\alpha^2 R_{PD}G_{PD}}{4R_L}|r(\omega_s)|^2\sin(\varphi) \tag{S24}$$

(S25)

It is then easy to see the reflection amplitude and phase are given by

$$|r(\omega_s)|^2 = \frac{4R_L}{a_o^2\alpha^2 R_{PD}G_{PD}}\sqrt{X|^2_{\omega_{\mathrm{LI}}} + Y|^2_{\omega_{\mathrm{LI}}}} \qquad \text{and} \qquad \tan(\varphi) = \frac{Y|_{\omega_{\mathrm{LI}}}}{X|_{\omega_{\mathrm{LI}}}}.$$

From the imparted change in the phase the signal delay is then calculated as:

$$\tau^{(\mathrm{R})} = \frac{\varphi}{\omega_{\mathrm{LI}}}$$

where $\tau^{(\mathrm{R})} > 0$ ($\tau^{(\mathrm{R})} < 0$) represent a delay (advance) on the signal.

Here we have neglected the gain provided by the lock-in, which is important to determine the absolute value of $r(\omega_s)$. To account for that we calibrate the X channel by a normalized transmission curve taken with low input power. Our assumption is that the cavity-taper coupling is not affected by the input power. A analogous result can be found for the case where the control laser is on the blue side of the cavity ($\omega_{\mathrm{c}} > \omega_o$).

Room-temperature Electromagnetically Induced Transparency

Reflection spectroscopy of the system at 296 K results in the spectra shown in Fig. S6. Due to the larger intrinsic mechanical damping rate at room temperature ($\gamma_i = 2\pi \times 1.9$ MHz), higher power is required to reach a given cooperativity. Additionally, the nanobeam optomechanical system is thermally sensitive and responds at a rate faster than the 89 kHz modulation signal used. As such, part of the phase response is thermal in nature. This added effect masks the small coherent phase-shifts imparted by the optomechanical cavity on the modulated signal sidebands. Nonetheless, the Fano resonances measured (See Fig. S6b) are a direct indication of coherent interference between the excitation of the optical cavity and the mechanical phonon.

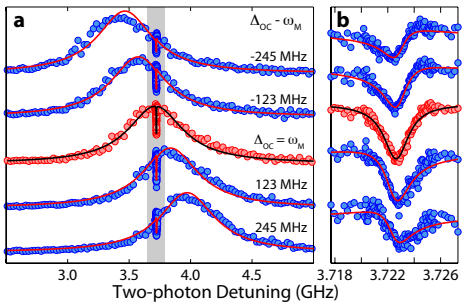

FIG. S6: **Room-temperature and amplification results. a,** room temperature normalized reflection signal from the probe laser as a function of the two photon detuning. Each curve represents a different control laser detuning from the optical cavity (Δ_{OC}). The transparency window data as well as the fitted curve is shown around the mechanical frequency in **b**.

---

* These authors contributed equally to this work.

[1] Agarwal, G. S. & Huang, S. Electromagnetically induced transparency in mechanical effects of light. *Physical Review A* **81**, 041803 (2010).
[2] Weis, S. *et al.* Optomechanically induced transparency. *Science* science.1195596 (2010).
[3] Fleischhauer, M., Imamoglu, A. & Marangos, J. P. Electromagnetically induced transparency: Optics in coherent media. *Rev. Mod. Phys.* **77**, 633–673 (2005).
[4] Lukin, M. D. Colloquium: Trapping and manipulating photon states in atomic ensembles. *Rev. Mod. Phys.* **75**, 457–472 (2003).
[5] Lezama, A., Barreiro, S. & Akulshin, A. M. Electromagnetically induced absorption. *Phys. Rev. A* **59**, 4732– (1999).
[6] Louisell, W. H., Yariv, A. & Siegman, A. E. Quantum fluctuations and noise in parametric processes. i. *Phys. Rev.* **124**, 1646– (1961).
[7] Yariv, A. Quantum theory for parametric interactions of light and hypersound. *Quantum Electronics, IEEE Journal* **1**, 28–36 (1965).
[8] Mollow, B. R. & Glauber, R. J. Quantum theory of parametric amplification. I. *Phys. Rev.* **160**, 1076– (1967).
[9] Aspelmeyer, M., Grblacher, S., Hammerer, K. & Kiesel, N. Quantum optomechanics throwing a glance [invited]. *J. Opt. Soc. Am. B* **27**, A189–A197 (2010).
[10] Borselli, M., Johnson, T. J. & Painter, O. Measuring the role of surface chemistry in silicon microphotonics (2006).